

# Moving Load-Structure Coupled Vibration Analysis and Vibration Isolation for Port Machinery



LU Kai-liang

# Vehicle-bridge Coupled Vibration

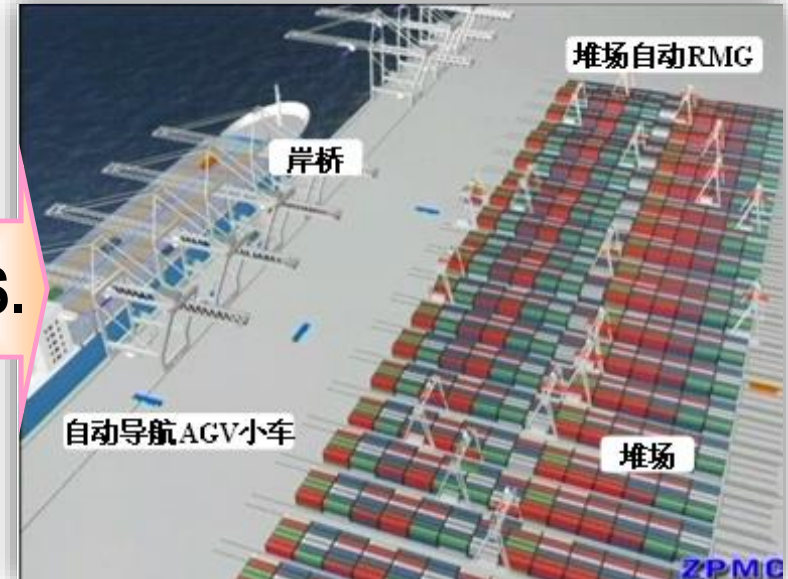
## II. PROJECT INTRODUCTION

### (1) Background

#### Horizontal Transport Schemes for Automated Container Terminal



**3D Distributing System  
with container vehicle-truss bridge**



**2D Automatic Guided Vehicle (AGV)  
System**

**V.S.**

Efficiency:	3D, no vehicle interference; Max. $V \geq 20\text{m/s}$ ; Wheel-rail positioning accuracy $\pm \text{cm}$	> AGVs conflict; Max. Velocity=20m/s; GPS positioning accuracy $\pm \text{mm}$
Cost:	Truss bridge, rail, electric vehicle—Low	< AGVs—High
Environment:	Friendly, no emission & low noise	= Friendly, no emission & low noise
Flexibility:	Low, fit for throughput constant terminal	< High

**Acknowledgements:** This research is sponsored and funded by the National “863” Key Project “Automated Container Terminal Equipment and Demonstrations”(Grant NO.2009AA043000).



# Vehicle-bridge Coupled Vibration II. PROJECT INTRODUCTION

## (2) Problem Definition



**EXCITATION** → **COUPLED SYSTEM** → **RESPONSE**

Self-excitation:

- track irregularity
- hunting movement

External excitation

- wind load
- seismic load

Container  
vehicle

Wheel-rail contact

Truss bridge

Vehicle-  
bridge  
Coupled  
Vibration  
Response

**ASSESSMENT**

Structural Safety

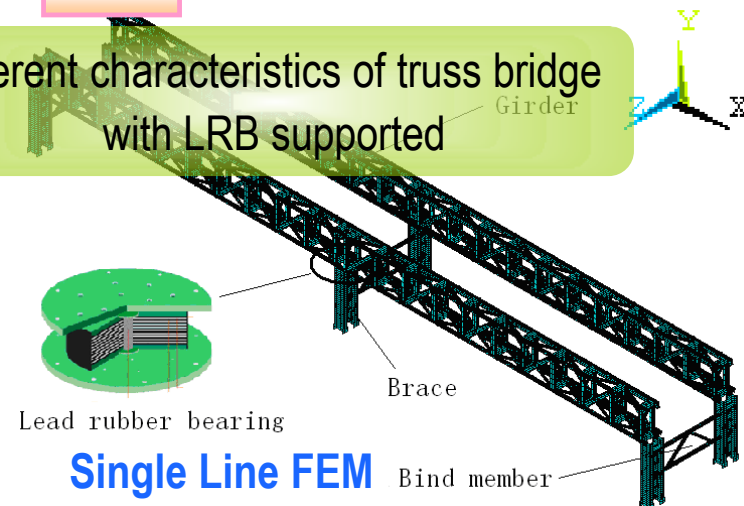
Running Stationarity



VR Simulation

Experimentation Line

Inherent characteristics of truss bridge  
with LRB supported



Single Line FEM

### (3)Solution & Method

- Stochastic excitation (**track irregularity**, fluctuating wind, etc)

numerical simulation with Shinozuka's method of multidimensional homogeneous process

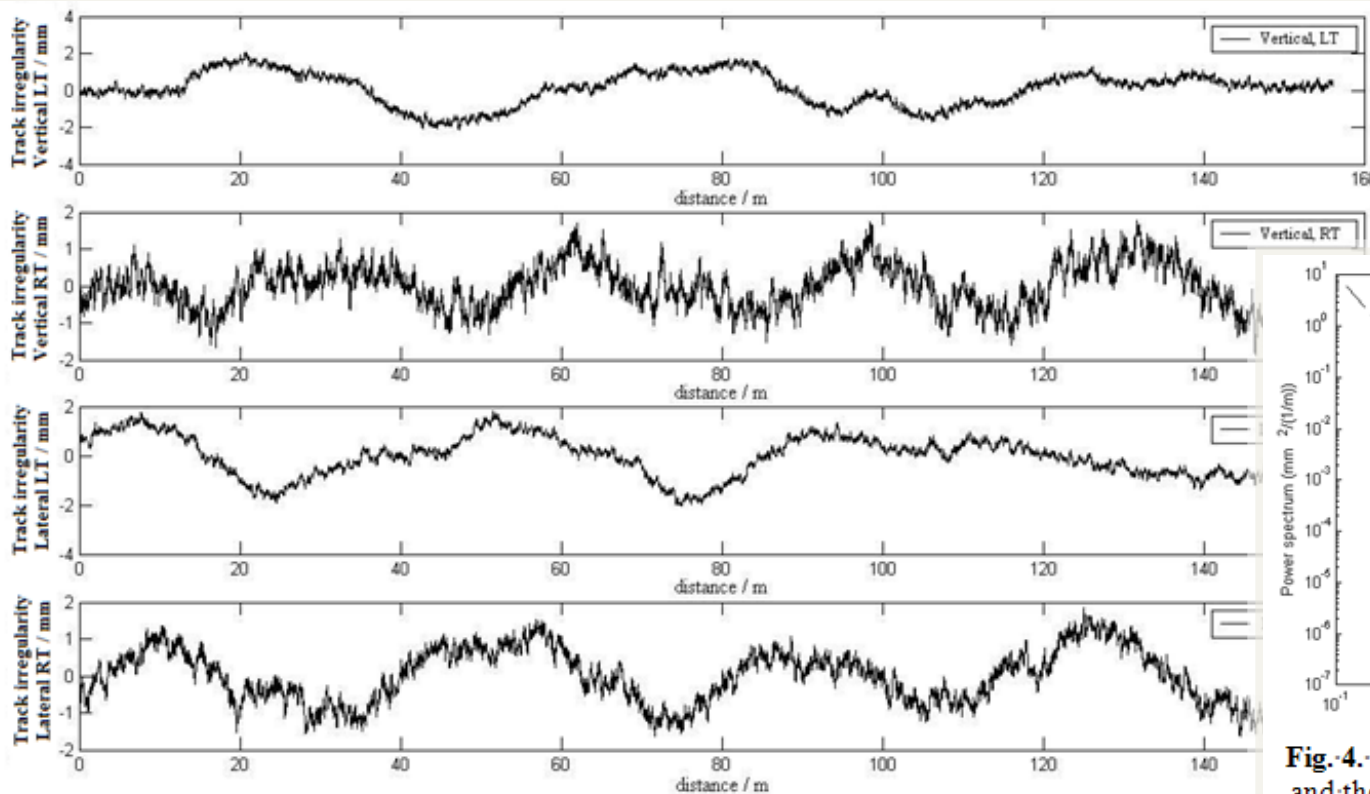


Fig. 3. Vertical and lateral track irregularity curve of the left and right track.

$$S(f) = \frac{A(f^2 + Bf + C)}{f^4 + Df^3 + Ef^2 + Ff + G}$$

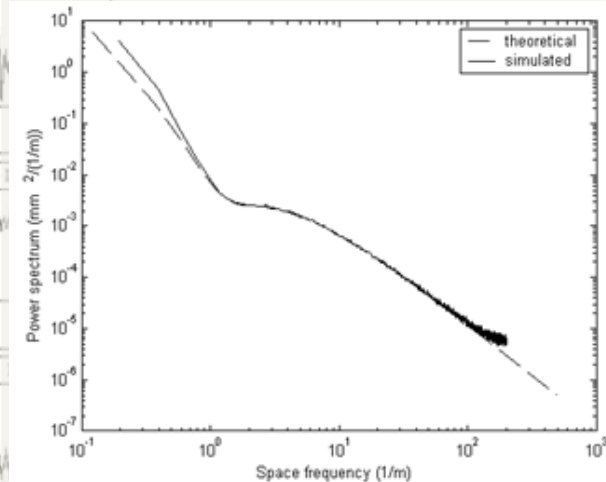
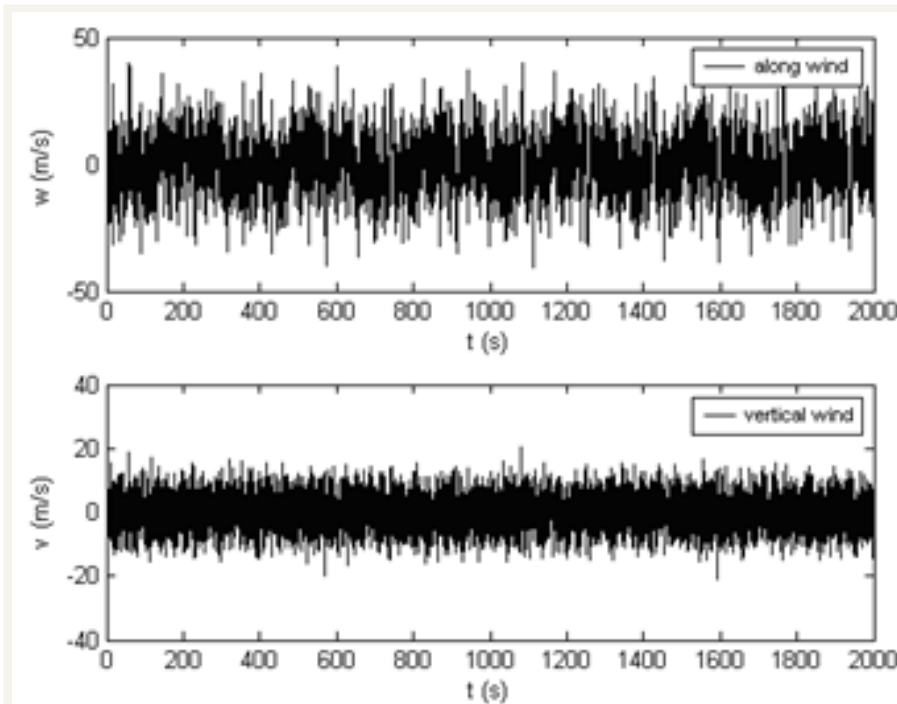


Fig. 4. Comparison of the theoretical spectrum and the simulated spectrum of the left track's vertical irregularity.

### (3)Solution & Method

- Stochastic excitation (track irregularity, **fluctuating wind**, etc)

numerical simulation to Shinozuka's method of multidimensional homogeneous process



**Fig. 5.** Time history of along-wind and vertical-wind fluctuating wind velocity ( $\bar{U}(10) = 60\text{m/s}$ )

Along wind direction:  
Kaimal spectrum

$$S_w(y, n) = \frac{200f \cdot u_*^2}{n(1 + 50f)^{5/3}}$$

Vertical wind direction:  
Lumley-Panofsky spectrum

$$S_v(y, n) = \frac{3.36f \cdot u_*^2}{n(1 + 10f^{5/3})}$$

### (3)Solution & Method

#### ■ Coupled dynamic equation of vehicle-bridge system

free-interface Component Modal Synthesis method; considering LRB as link substructure, then Super-element Indirect CMS Method can be derived.

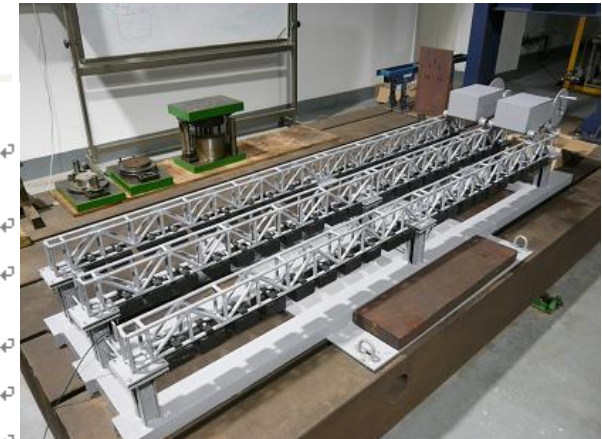
(FOR DETAIL PI. REFER TO Appendix B or “reference paper 2.pdf”. )

### (4)Result & Discussion

#### ■ Self-excitation response and scale model test validation

**Table 3.** Maximum acceleration response comparison of model test and prototype simulation

Prototype Vehicle Speed (m/s)	Support Form	Maximum Acceleration Response of Bridge (m/s <sup>2</sup> )				Maximum Acceleration Response of Vehicle (m/s <sup>2</sup> )			
		Vertical		Lateral		Vertical		Lateral	
		Test	Simulation	Test	Simulation	Test	Simulation	Test	Simulation
4	rigid	2.05	1.54	0.15	0.16	0.26	0.069	0.32	0.220
	flexible	1.37	1.32	0.14	0.12	0.22	0.063	0.29	0.218
6	rigid	2.07	1.60	0.20	0.20	0.38	0.129	0.61	0.410
	flexible	1.70	1.34	0.16	0.15	0.41	0.126	0.48	0.397
8	rigid	2.23	1.65	0.19	0.24	0.49	0.223	0.81	0.634
	flexible	1.80	1.38	0.18	0.20	0.55	0.238	0.73	0.576

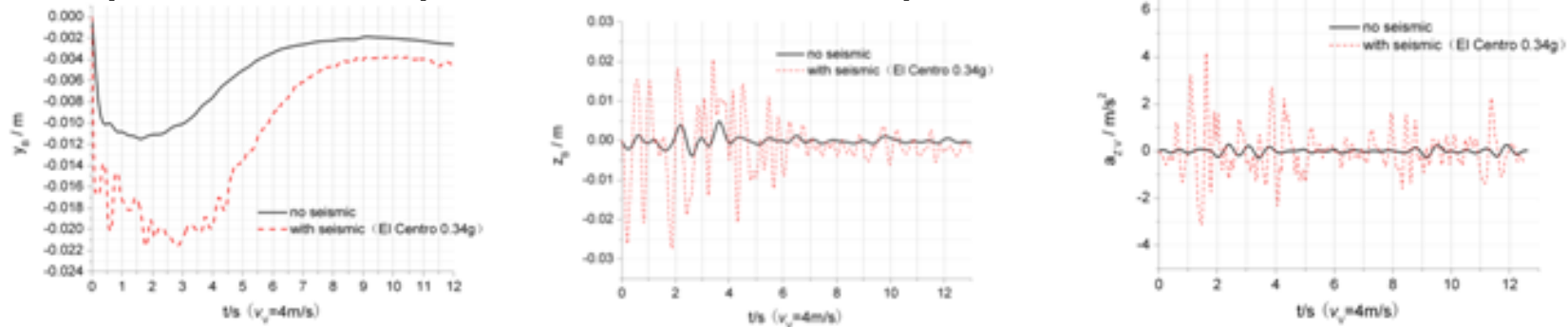


**1:30 Scaled Vehicle-bridge Model**



### (4)Result & Discussion

#### ■ Coupled vibration response under seismic and operational wind load



a) Vertical displacement

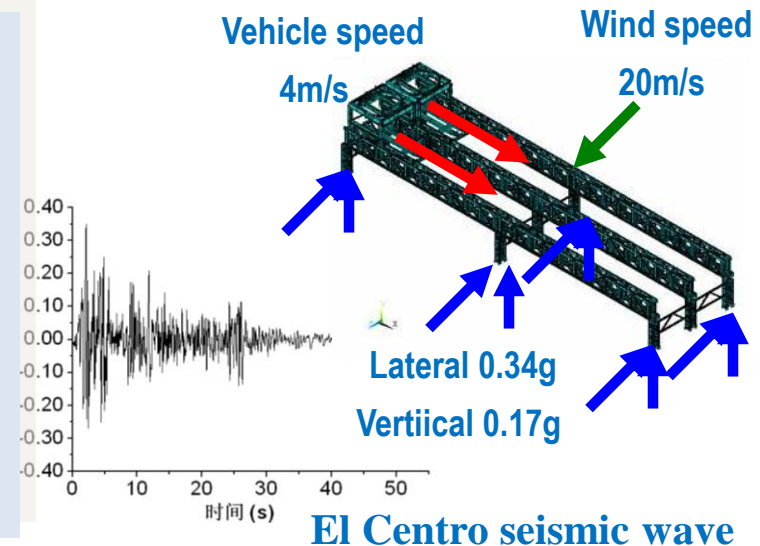
b) Lateral displacement

c) Lateral acceleration

**Fig.10.** The dynamic response comparison of the vehicle-bridge vibration under either seismic load or not

**Remarks:** (1)when seismic load applied, the maximum response and frequency value become larger than that without earthquake load. The displacement and acceleration in middle span under seismic load is 1.9, 4.6 and 12.4 times than that without.

(2)Furthermore, vertical displacement time-history in middle span presents moving vehicle load is significant for the coupled vibration and that seismic load mainly affects the amplitude. However, in lateral vibration analysis, all time-history curve is similar to El Centro wave, which means that seismic load is main cause, compared to operational wind load and self-excitation.



El Centro seismic wave

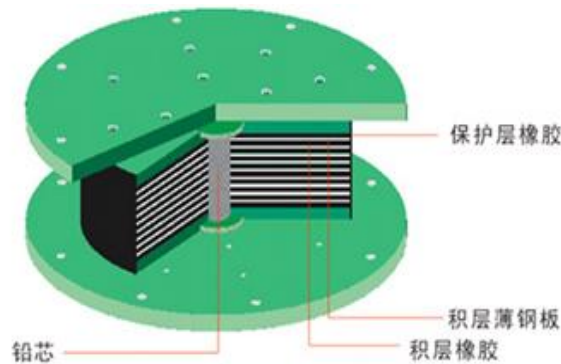
### Representative published papers:

- [1] **Real-time simulation dynamics model and solution algorithm for the trolley-hoisting system in container crane simulated training system**[J]. JVE, Vol.17, No.3, 2016.(SCI)
- [2] Container Vehicle-Truss Bridge Coupled Vibration Analysis and Structural Safety Assessment under Stochastic Excitation[J]. Journal of Vibroengineering. Vol. 16, No.5, pp3122-3136, 2014. (SCI)
- [3] **Crack Analysis of Multi-plate Intersection Welded Structure in Port Machinery Using Finite Element Stress Calculation and Acoustic Emission Testing**[J]. IJHIT: International Journal of Hybrid Information Technology, Vol. 7, No. 5, pp323-340, 2014. (EI)
- [4] Joint Simulation of Trolley Vehicle-Frame Structure Coupled Vibration Using ADAMS and ANSYS for Container Crane Simulated Training System, IJHIT: International Journal of Hybrid Information Technology, Vol. 6, No. 5., 2013. (EI)
- [5] Vibration Rapid Analysis and Comparison of Motor Support in Container Crane's Machine Room with Single Degree of Freedom and Finite Element Method Based on Visual Basic, International Journal of Grid and Distributed Computing, Vol. 6, No. 4, pp. 75-84, 2013. (EI)
- [6] Container Vehicle-Truss Bridge Coupled Vibration Analysis under Wind and Seismic Load[J]. Engineering Mechanics, 29 (10): 288-293, 2012. (EI)
- [7] **Anti - seismic Device Design and Model Test Validation for Container Crane**[J]. Journal of Vibration, Measurement & Diagnosis, 31(4): 501-506, 2011. (EI)
- [8] Wind-induced Lateral Vibration of a 7500t Floating Crane's Boom Considering Axial Clearance between Boom and Pin Hinge[J]. Journal of Vibration and Shock, 28(10): 94-98, 2009. (EI)



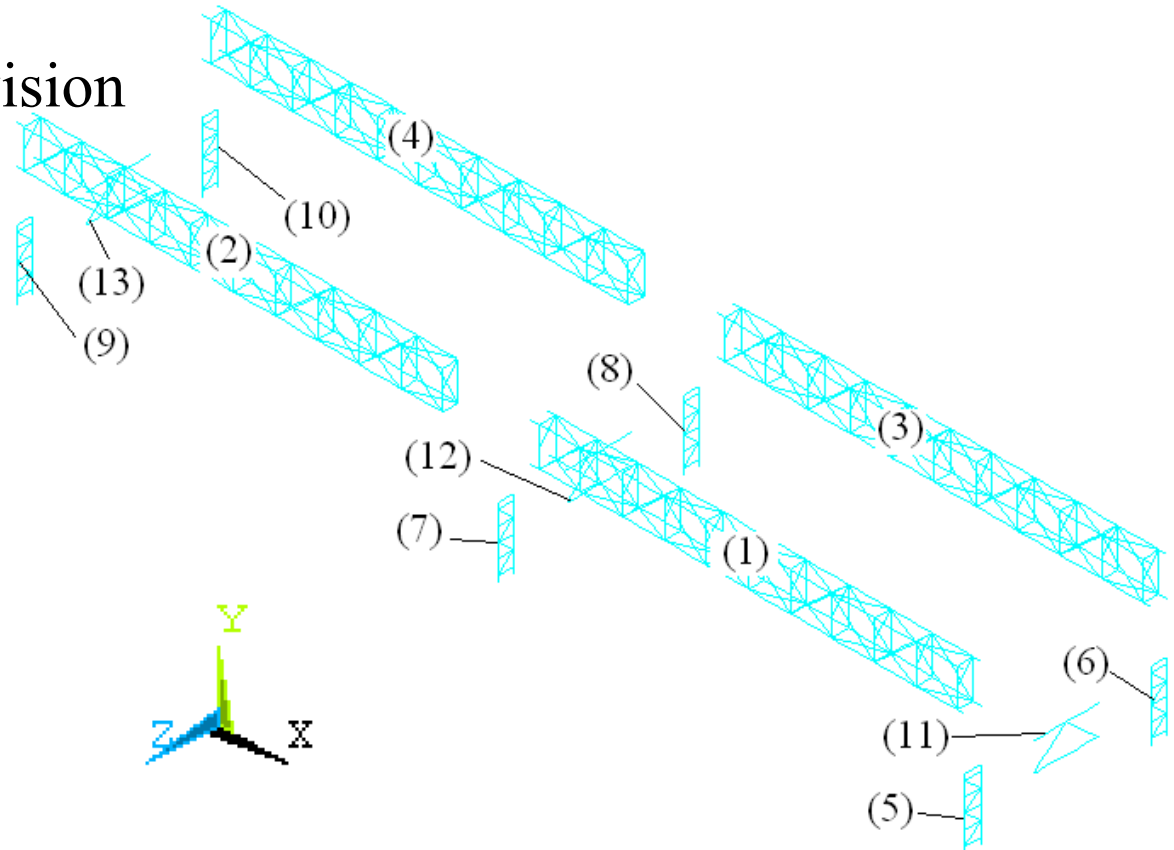
## 2 Super-element indirect CMS by Guyan static condensation

### ● 2.1 Substructure's division



LRB as

Link substructure



Girder, Brace, Bind member as

Free-interface substructure

## • 2.2 The first coordinate transformation for substructures

### (1) Free-interface substructure

Use the assumed branch mode set  $\Phi$ , composed of first- $k$ -order normal modes  $\Phi_k$  and residual attachment modes  $\Psi_d$  as the transformation matrix.

Through the regularization of mode to mass matrix, the stiffness matrix and mass matrix of free-interface substructure in modal coordinates can be derived as

$${}^A\bar{\mathbf{k}} = \begin{bmatrix} {}^A\mathbf{A}_{kk} & \\ & {}^A\Psi_d^T {}^A\mathbf{k} {}^A\Psi_d \end{bmatrix} \quad {}^A\bar{\mathbf{m}} = \begin{bmatrix} {}^A\mathbf{I}_{kk} & \\ & {}^A\Psi_d^T {}^A\mathbf{m} {}^A\Psi_d \end{bmatrix}$$

### (2) Super-element link substructure

Set the stiffness and mass matrixes of link substructure under master coordinate  ${}^E\mathbf{u}_m$  and slave coordinate  ${}^E\mathbf{u}_s$  as

$${}^E\mathbf{k} = \begin{bmatrix} {}^E\mathbf{k}_{ss} & {}^E\mathbf{k}_{sm} \\ {}^E\mathbf{k}_{ms} & {}^E\mathbf{k}_{mm} \end{bmatrix} \quad {}^E\mathbf{m} = \begin{bmatrix} {}^E\mathbf{m}_{ss} & {}^E\mathbf{m}_{sm} \\ {}^E\mathbf{m}_{ms} & {}^E\mathbf{m}_{mm} \end{bmatrix}$$

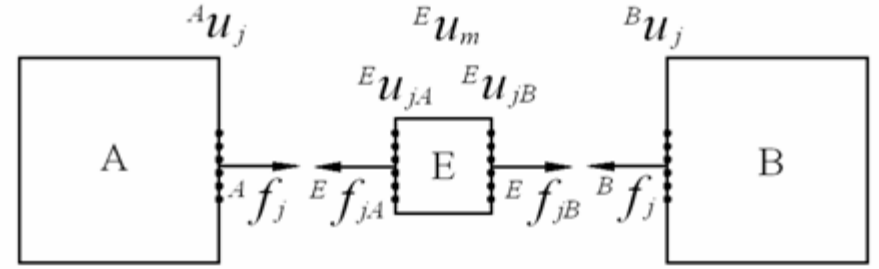


Figure 1: Sketch map of substructure interface connection

By **Guyan static condensation**, the stiffness and mass matrixes only under interface DOF is

$${}^E\tilde{\mathbf{k}} = {}^E\boldsymbol{\Psi}_c^T {}^E\mathbf{k} {}^E\boldsymbol{\Psi}_c \quad {}^E\tilde{\mathbf{m}} = {}^E\boldsymbol{\Psi}_c^T {}^E\mathbf{m} {}^E\boldsymbol{\Psi}_c$$

in which,  ${}^E\boldsymbol{\Psi}_c$  is **static transformation matrix**

$${}^E\boldsymbol{\Psi}_c = \begin{bmatrix} -{}^E\mathbf{k}_{ss}^{-1} {}^E\mathbf{k}_{sm} & \mathbf{I} \end{bmatrix}^T$$

Since  ${}^E\mathbf{u}_m = \begin{bmatrix} {}^E\mathbf{u}_{jA} & {}^E\mathbf{u}_{jB} \end{bmatrix}^T$ , the above equation can be written in block form:

$${}^E\tilde{\mathbf{k}} = \begin{bmatrix} {}^E\tilde{\mathbf{k}}_{(jA)(jA)} & {}^E\tilde{\mathbf{k}}_{(jA)(jB)} \\ {}^E\tilde{\mathbf{k}}_{(jB)(jA)} & {}^E\tilde{\mathbf{k}}_{(jB)(jB)} \end{bmatrix} \quad {}^E\tilde{\mathbf{m}} = \begin{bmatrix} {}^E\tilde{\mathbf{m}}_{(jA)(jA)} & {}^E\tilde{\mathbf{m}}_{(jA)(jB)} \\ {}^E\tilde{\mathbf{m}}_{(jB)(jA)} & {}^E\tilde{\mathbf{m}}_{(jB)(jB)} \end{bmatrix}$$

### ● 2.3 Assemble system equation & the second coordinate transformation

After the first coordinate transformation, the system's non-damping vibration equation, under the coordinate  $\mathbf{p} = \begin{bmatrix} {}^A\mathbf{p}_k & {}^A\mathbf{f}_j & {}^E\mathbf{u}_{jA} & {}^E\mathbf{u}_{jB} & {}^B\mathbf{p}_k & {}^B\mathbf{f}_j \end{bmatrix}^T$ , is

$$\mathbf{m}\ddot{\mathbf{p}} + \mathbf{k}\mathbf{p} = \mathbf{0}$$

$$m = \begin{bmatrix} {}^A\boldsymbol{I}_{kk} & & & & & \\ & {}^A\boldsymbol{\Psi}_d^T {}^Am {}^A\boldsymbol{\Psi}_d & & & & \\ & & {}^E\tilde{m}_{(jA)(jA)} & {}^E\tilde{m}_{(jA)(jB)} & & \\ & & {}^E\tilde{m}_{(jB)(jA)} & {}^E\tilde{m}_{(jB)(jB)} & & \\ & & & & {}^B\boldsymbol{I}_{kk} & \\ 0 & & & & & {}^B\boldsymbol{\Psi}_d^T {}^Bm {}^B\boldsymbol{\Psi}_d \end{bmatrix}$$
$${}^E \mathbf{u}_{jA} = {}^A \mathbf{u}_j \quad {}^E \mathbf{u}_{jB} = {}^B \mathbf{u}_j$$
$${}^E \mathbf{f}_{jA} = -{}^A \mathbf{f}_j \quad {}^E \mathbf{f}_{jB} = -{}^B \mathbf{f}_j$$
$$\begin{Bmatrix} {}^A \mathbf{p}_k \\ {}^A \mathbf{f}_j \\ {}^E \mathbf{u}_{jA} \\ {}^E \mathbf{u}_{jB} \\ {}^B \mathbf{p}_k \\ {}^B \mathbf{f}_j \end{Bmatrix} = \begin{bmatrix} \mathbf{I} & \mathbf{0} & \mathbf{0} & \mathbf{0} \\ \mathbf{0} & \mathbf{0} & \mathbf{I} & \mathbf{0} \\ {}^A \boldsymbol{\Phi}_{jk} & \mathbf{0} & {}^A \boldsymbol{\Psi}_{jd} & \mathbf{0} \\ \mathbf{0} & {}^B \boldsymbol{\Phi}_{jk} & \mathbf{0} & {}^B \boldsymbol{\Psi}_{jd} \\ \mathbf{0} & \mathbf{I} & \mathbf{0} & \mathbf{0} \\ \mathbf{0} & \mathbf{0} & \mathbf{0} & \mathbf{I} \end{bmatrix} \begin{bmatrix} \mathbf{I} \\ -\mathbf{C}_{dd}^{-1} \mathbf{C}_{kk} \end{bmatrix} \begin{Bmatrix} {}^A \mathbf{p}_k \\ {}^B \mathbf{p}_k \end{Bmatrix} = \mathbf{T}_2 \mathbf{T}_3 \begin{Bmatrix} {}^A \mathbf{p}_k \\ {}^B \mathbf{p}_k \end{Bmatrix} = \mathbf{T} \begin{Bmatrix} {}^A \mathbf{p}_k \\ {}^B \mathbf{p}_k \end{Bmatrix}$$



Eliminating non-independent DOFs, thus can obtain system's equation of free vibration under the approximate space of **generalized coordinate**  $\mathbf{q} = \begin{bmatrix} {}^A \mathbf{p}_k & {}^B \mathbf{p}_k \end{bmatrix}^T$ , which is given by

$$\mathbf{M} \ddot{\mathbf{p}}_k + \mathbf{K} \mathbf{p}_k = \mathbf{0} \quad \mathbf{M} = \mathbf{T}^T \mathbf{m} \mathbf{T} \quad \mathbf{K} = \mathbf{T}^T \mathbf{k} \mathbf{T}$$

### ● 2.4 Inverse transform to physical coordinates

For **free-interface substructure**

$$\mathbf{u} = \begin{bmatrix} {}^A \mathbf{u} & {}^B \mathbf{u} \end{bmatrix}^T = \mathbf{T}_4 \mathbf{T}_3 \mathbf{q} \quad \mathbf{T}_4 = \begin{bmatrix} {}^A \Phi_{ik} & {}^B \Phi_{ik} & {}^A \Phi_{jk} & {}^B \Phi_{jk} \\ {}^A \Psi_{id} & {}^B \Psi_{id} & {}^A \Psi_{jd} & {}^B \Psi_{jd} \end{bmatrix}^T$$

For **link substructure**

$${}^E \mathbf{u} = {}^E \Psi_c \mathbf{T}_1 \mathbf{T}_3 \mathbf{p}_k$$

### 3 Super-element indirect CMS by **dynamic** condensation (omitted)

## Summary

- The super-element indirect CMS deduced will eventually solve system's dynamic problem in the approximate space which is set out by the normal mode coordinates of every free-interface substructure, which reduces system's DOF enormously.
- Because the generalized coordinates of link substructure don't take part in constructing approximate solving space. In that case, when there are non-linear elements in link substructure, we only need to modify the coordinate transformation matrix to modify system's generalized  $k$ ,  $c$  and  $m$  matrix. Therefore, the computational efficiency improves.
- On the other hand, the introduction of super-element link substructure can handle components' structural damping and connectors' lumped damping separately and then couple into the entire system, which is better than Raleigh damping, especially for some devices with concentrated damping such as rubber bearings, dampers and so on.

*Thanks for your attention!*